Proceedings of the ASME 2010 3rd Joint US-European Fluids Engineering Summer Meeting and 8th International Conference on Nanochannels, Microchannels, and Minichannels
FEDSM-ICNMM2010
August 1-5, 2010, Montreal, Canada

FEDSM-ICNMM2010-30881

EXPERIMENTAL INVESTIGATION OF THE MEAN CONCENTRATION FIELDS IN A COUNTERFLOWING JET

Luis A. Torres
Graduated Student
The University of Alberta
Edmonton, Alberta, Canada

Brian A. Fleck
Associate Professor
The University of Alberta
Edmonton, Alberta, Canada

David J. Wilson
Retired Professor
The University of Alberta
Edmonton, Alberta, Canada

David Nobes
Assistant Professor
The University of Alberta
Edmonton, Alberta, Canada

Mohammad Mahmoudi
Graduate Student
The University of Alberta
Edmonton, Alberta, Canada

ABSTRACT

The geometrically similar region of the centerline concentration decay of a counter-flowing jet was investigated using planar laser induced fluorescence. The jet is investigated for jet to counterflowing velocity ratios (U_r) in the range $4<U_r<19$. New length scales for this flow were studied and used to generate empirical expressions to predict the concentration decay in the established flow zone. These length scales were defined using the 5% contour of the mean concentration field of the counterflowing jet. Additional experiments for two jet to counterflow velocity ratios were used to validate these empirical expressions. The new empirical expressions correlate well with the concentration decay in the centerline of the counterflowing jet within the free jet-like region. It was found that for some cases, the centerline concentration decay of the counterflowing jet was better predicted considering decay proportional to $x^{-6/5}$, even though it can also be predicted by assuming decay with x^{-1}.

KEYWORDS

Counterflow, Jet, Concentration, PLIF.

INTRODUCTION

Though turbulent jets are probably one of the most studied of shear flows, few investigations on the flow characteristics of a round jet issuing into a uniform counterflow stream apper in the literature (Arendt et al., 1956; Sui, 1961; Timma, 1962; Beltaos and Rajaratnam, 1973; Morgan and Brinkworth, 1976; McDannel et al., 1982; Konig and Fiedler, 1991b; Konig and Fiedler, 1991a; Lam and Chan, 1995; Yoda and Fiedler, 1996; Lam and Chan, 1997; Chan and Lam, 1998; Lam and Chan, 2002; Bernero and Fiedler, 2000; Tsunoda and Saruta, 2003). This is true, even considering how counterflowing jets can be found in several industrial and environmental fluid applications (Lam and Chan, 1995). They have been used for the stabilization in afterburners of turbojet engines as well as an enhancer for dispersion and mixing process (Beltaos and Rajaratnam, 1973; Chan, 1999). The mean flow geometrical parameters for a counterflowing jet are shown in Figure 1. The flow of a counterflowing jet is generated by a nozzle of diameter D with a velocity Uj, and in some cases the jet carries a scalar concentration (Cj). Once the jet is in contact with the uniform counterflow stream, with velocity U_o, the mixing process begins.This mixing process creates a decay of the concentration downstream the exit of the jet. In this process there is a momentum exchange, where the uniform counterflow stream is able to stop the flow of the jet that is then carried back with the counter current (Yoda and Fiedler, 1996). The distance from the exit of the jet to the point where zero velocity is reached is known as the jet penetration length (x_p), which also defines the location of the stagnation streamsurface at the centerline of the jet. Figure 1 also shows three regions downstream from the jet exit. The zone of flow establishment (ZFE) contains the iso-concentration core and the transition to the established flow region (EFR). In the EFR the jet flow is the dominant flow and the counterflowing jet behaves similar to a free jet in quiescent surrounding (Konig and Fiedler, 1991b; Beltaos et al., 1999; Yoda and Fiedler, 1996). Finally,

one can see the mixing zone (MZ) where the flow is dominated by the counterflow stream.

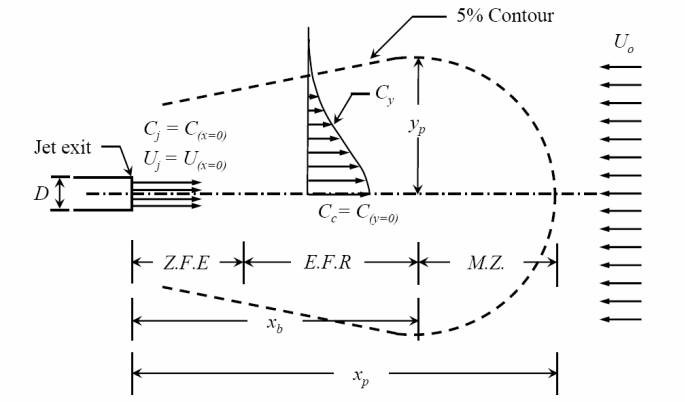

Figure 1: A conceptual schematic of the flow field (after Beltaos and Rajaratnam (1973), Yoda and Fiedler (1996), and Chan (1999)).

Among the few investigations carried out related to the counterflowing jet, the penetration distance and the centerline velocity decay have been the primary focus. The axial penetration distance of a counterflowing jet has been sufficiently studied for different jet to counterflow velocity ratios *(U_r)*. The studied values of U_r go from 1.3 to 15 (Beltaos and Rajaratnam, 1973; Morgan and Brinkworth, 1976; Konig and Fiedler, 1991b; Yoda and Fiedler, 1996; Lam and Chan, 1997). These investigations lead to the conclusion that the jet penetration was governed by U_r. It was found that the penetration length had a linear relationship with the velocity ratio. Morgan and Brinkworth (1976) established that this linear relation between the jet penetration and the velocity ratio is valid just for velocity ratios within the "low momentum region". This region is found where the ratio of momentum fluxes is less than 0.5, for higher ratios of momentum fluxes the relationship between jet penetration and velocity ratio is not longer linear. Beltaos and Rajaratnam (1973) studied the velocity scale along the centerline of the counterflowing jet using the penetration length *(x_p)* as the geometrical scale for the axial velocity decay. Using x_p as the axial scale for the velocity Beltaos and Rajaratnam (1973) demonstrated that the profiles of the centerline velocity collapsed on a single curve for jet to counterflow velocity ratios higher than 4. In the discussion presented by Beltaos et al. (1999) it was found that this universal form of the centerline velocity decay was valid just for axial distances greater than half the total jet penetration, a finding that was supported by the investigation of Chan and Lam (1998). Chan and Lam (1998) presented an investigation of the centerline velocity decay of a counterflowing jet where an analytical model was presented to predict the centerline velocity based on the conservation of mass flux and momentum flux. An analytical model was also presented by Chan (1999) for the centerline concentration decay of a counterflowing jet; this model was obtained based on the velocity field of the counterflowing jet. To the knowledge of the author, no further attempt has been made in order to define new length scales for the centerline concentration decay in a counterflowing jet. Therefore, this chapter presents a study on new length scales for the centerline concentration decay of the counterflowing jet throughout planar laser induced fluorescence. Forms of the aspect ratio of the 5% contour are used as length scales for the center-line concentration decay. These scaling factors are used to generate simple empirical expressions to predict the concentration decay of the counterflowing jet. These expressions are validated with additional experimental data of the mean concentration field of the counterflowing jet.

NOMENCLATURE

C	fluorescein concentration, mg.L^{-1}
C_c	concentration at the centerline of the jet, mg.L^{-1}
C_j	concentration at the exit of the jet, mg.L^{-1}
C_x	mean concentration along the x axis, mg.L^{-1}
C_y	mean concentration along the y axis, mg.L^{-1}
D	internal jet diameter, mm
Re_D	diameter based Reynolds number
U	horizontal velocity component, cm.s^{-1}
U_f	velocity of the dyed fluid, cm.s^{-1}
U_j	velocity of the jet, cm.s^{-1}
U_o	velocity of counterflow stream, cm.s^{-1}
U_r	jet to counterflow velocity ratio
x_p	maximum axial penetration length, mm
y_p	maximum lateral penetration length, mm
x_b	axial location of the maximum lateral penetration length, mm
λ	length ratio (y_p/x_b)
β	length ratio (y_p/x_p)
φ	Length ratio (x_b/x_p)

EXPERIMENTAL SETUP

The experiments were carried out in a closed loop water channel facility in the Mechanical Engineering Department at the University of Alberta. The water channel has a cross section of 680 mm by 480 mm, and the total length of the water channel is approximately 5000 mm, see figure 2. The jet was produced by using two cylindrical nozzles with an internal diameter of 8.841 and 5.64 mm, hereafter referred to as D_1 and D_2 respectively. These jets were fed from a pressurized stainless steel tank and the gauge pressure in the tank was kept constant at 206.84 kPa. Both jets were designed to have an inlet length of 104D with the aim of having a fully developed flow. The velocity of the jet was controlled by a valve located far upstream the inlet of the jet. The counterflowing jet was located at the center of the test section. The test section was located 3200 mm downstream from the inlet of the water channel. The jet was set at approximately 200 mm from the bottom of the water channel in the test section, and the level of water was kept constant at a height of 400 mm for all the experiments. Different jet to counterflow velocity ratios were tested for the

two jet diameters, the velocity of the counterflow stream was kept at a constant value of 5 cm.s^{-1} as the velocity of the jet was adjusted to obtain the desired jet to counterflow velocity ratio. Table 1 summarizes the initial jet condition used in the experiments.

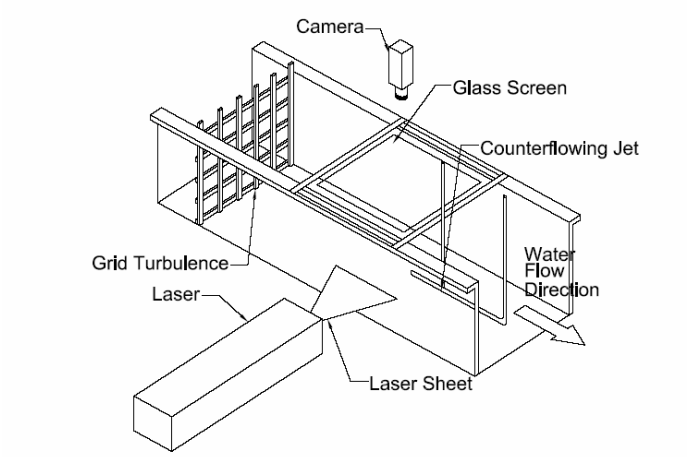

Figure 2: The schematic of the experimental setup.

Table 1: Jet parameters that used in the experiments.

Re_D	U_r	U_j (m.s^{-1})	D (mm)
1580	4	0.18	8.81
3330	8	0.38	8.81
4640	11	0.53	8.81
5430	12	0.62	8.81
5870	14	0.67	8.81
2130	8	0.38	5.64
2970	11	0.53	5.64
3810	14	0.68	5.64
4540	16	0.81	5.64
5270	19	0.94	5.64

A uniform grid was place at the inlet of the water channel built with flat stainless steel bars of 19.2 by 5 mm of cross section area. The total open area was approximately 56 % with a mesh spacing of 76.2 mm. This grid turbulence generates near uniform velocity profile for the streamwise component, with variations found to be within 5 % (Hilderman, 2004). At the test section the turbulence intensity was found to be about 4 % for the mean horizontal (Hilderman, 2004).

The axial *(x)* mean scalar concentration fields were measured using planar laser induced fluorescence. The dye used for the scalar concentration measurements was fluorescein sodium salt, this dye was added and mixed in the stainless steel tank used to feed the nozzle. The concentration used in all the experiments was 0.05 mg.L^{-1}. The planar laser induced fluorescence system uses an optical arrangement that includes a Powell lens® to generate an approximately uniform thin laser sheet (Powell, 1987). Figure 2 depicts the experimental set-up used at the test section. A glass screen placed on the free surface was used to avoid any distortion due to the small waves. The camera was placed at approximately 1200 mm from the axis of the jet.

The laser used in this investigation was a 2.1 W Argon ion laser, which was operated in a single mode at a wavelength of 488 nm. A calibration process was employed before every experiment in order to obtain the scalar concentration field out of digital imaging analysis. Calibration images were obtained by traversing a glass square tube with a known dye concentration along the field of view of the camera while a set of images were being taken. The final calibration images were obtained by taking the average value of the sequence of instantaneous images at the known concentration. A linear fit was used to convert the fluorescent intensity into scalar concentration data. Instantaneous concentration images were recorded using a 12 bit SensiCam high speed CCD system, with a resolution of 1280 × 1024 pixels. At every flow jet condition a set of 500 images as taken at a rate of 19.32 Hz, with the exposure time used in each images of 10 ms. The spatial resolution established for the experiments was approximately 0.3 mm.pixel^{-1}.

RESULTS AND DISCUSSION

Figure 3 shows the average concentration field images for jet to counterflow velocity ratios (U_r) of 4, 8, 11, and 14 for the case of large jet diameter (D_1). Based on previous investigations it is expected that the mean axial penetration of the jet increases proportionally with the jet to counterflow velocity ratio (Rajaratnam, 1976; Konig and Fiedler, 1991b). Figure 4 depicts x_p plotted as a function of U_r. The data shown in this graph correspond to four different experiments, three of the which were done using a jet with diameter *D1* and one with D_2. From this figure it is possible to appreciate that the data fit relatively well the linear relation presented by Rajaratnam (1976) and Yoda and Fiedler (1996). Rajaratnam (1976) define the maximum penetration of the the jet as the point of the stagnation surface at the axis of the jet, meanwhile Yoda and Fiedler (1996) defined x_p as the maximum axial penetration distance of the mean fluorescence intensity field. In this investigation the maximum extension of the 5 % jet concentration contour at the center line of the jet was observed to agree with the linear relation found by Rajaratnam (1976) and Yoda and Fiedler (1996). Therefore, the geometrical length and scaling factors were defined using the contour of the 5 % concentration at the exit of the jet nozzle. The geometric length parameters in the jet were computed by considering the 5% contour of the concentration at the exit of the jet.

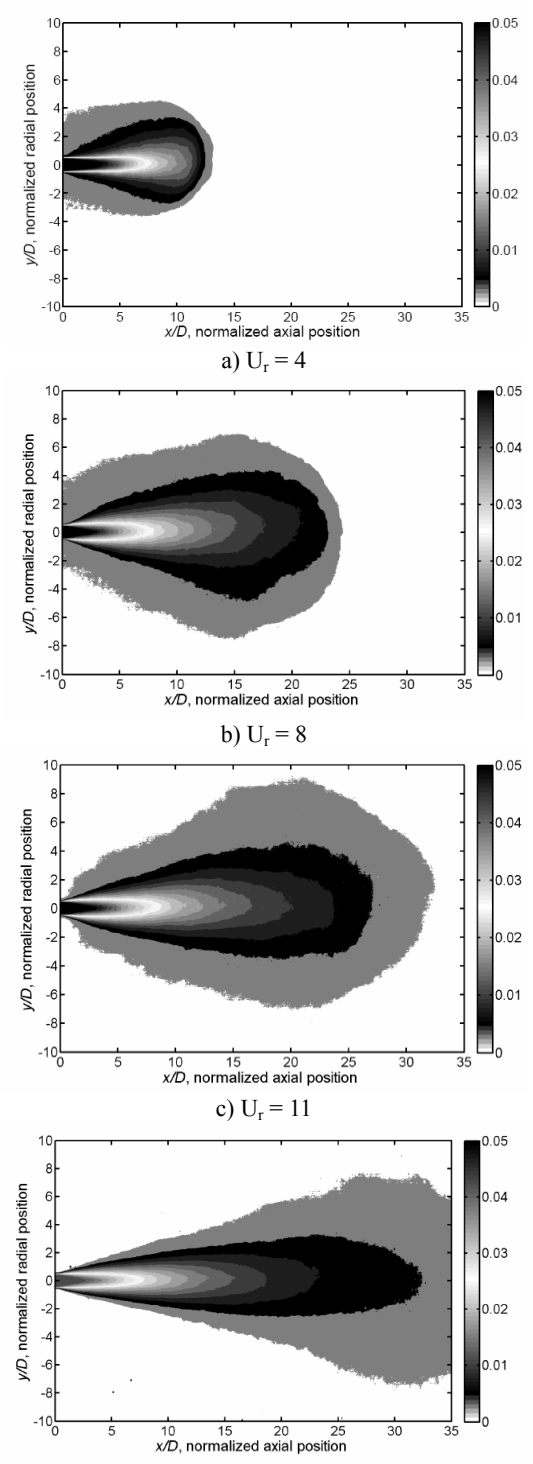

a) $U_r = 4$

b) $U_r = 8$

c) $U_r = 11$

d) $U_r = 14$

Figure 3: Time average of the scalar concentration field.

An example of the measurements for the different geometrical lengths for the counterflowing jet is given in Figure 5. In this figure it is possible to observe that the shape of the 5% contour is not symmetric along the axis of the jet, therefore, the maximum lateral penetration is not the same in both directions, the maximum discrepancy was found to be approximately 20% for the worst case. Consequently, the value of y_p will be determined by considering the average of the maximum penetration in both directions, this is the maximum half-width of the 5% contour.

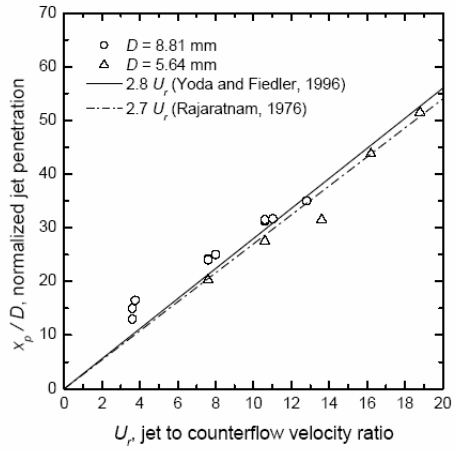

Figure 4: mean axial penetration of the counterflowing jet

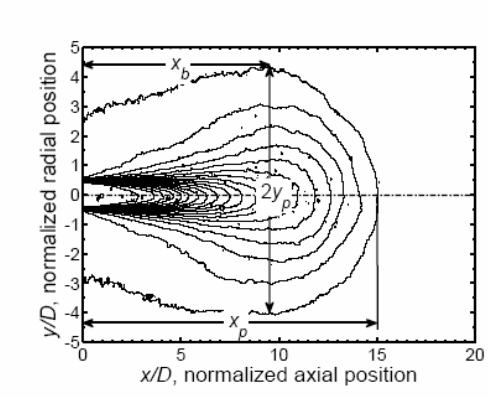

Figure 5: Example of the length parameters measured using the 5 % concentration contour.

The velocity ratios studied were contained within the "unstable case" defined by Konig and Fiedler (1991b), this is, for U_r greater than 1.4. In fact, some fluctuations of the jet were observed during the execution of the experiments. These fluctuations were found to be presented along, around, and across the axis of the jet, and were also pointed out in the studies presented by Yoda and Fiedler (1996) and Lam and Chan (1997). The fluctuations along the axis of the jet were observed through the execution of the experiments, and the larger variations were found for greater values of U_r. For instance, at $U_r = 14$ the axial penetration of the jet was found to fluctuate between 20D and 44D for a mean axial penetration of 40D. Throughout the experiments it was possible to observe that the shortest axial penetration was registered when the jet was bent out of the plane of the laser as well as a few times in the same plane. Figure 6a depicts an example of a bent jet in the same plane of the laser sheet which corresponds to the

shortest axial penetration of the jet for U_r = 8. The longest instantaneous penetration was found to be approximately 20% greater than the mean penetration. The longest instantaneous penetration was found usually when the jet flow was able to penetrate into the counterflow stream following an approximately straight path, which can be seen in Figure 6b.

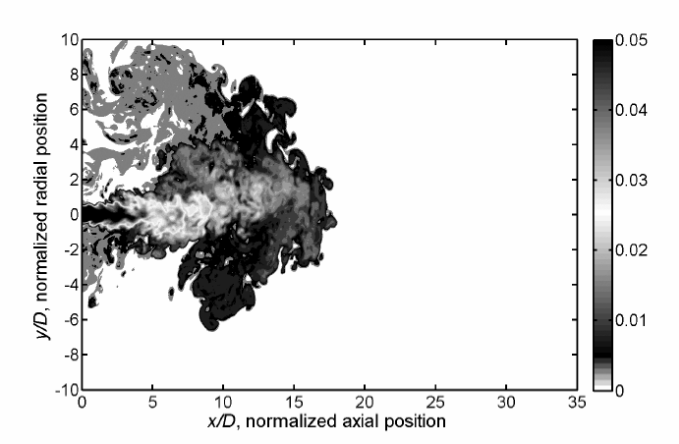

(a): The shortest penetration.

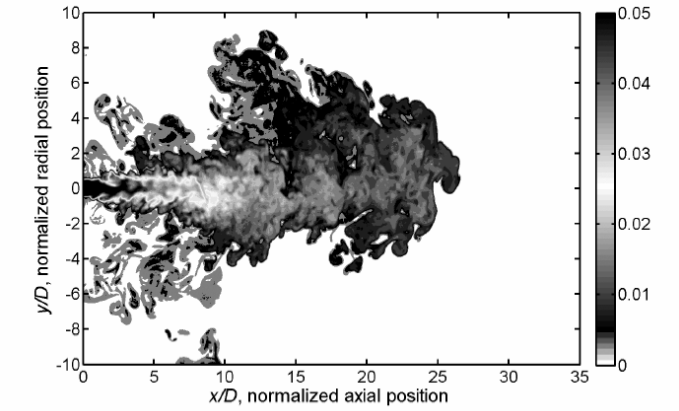

(b): The longest penetration.

Figure 6: Instantaneous scalar concentration field, $U_r = 8$.

Figure 7 depicts the centerline concentration decay for the counterflowing jet with a nozzle diameter of 8.81 mm. From this figure it is possible to appreciate the different length of the established flow region in the counterflowing jet its relationship with U_r.

The iso-concentration core region is characterized by having an approximately constant value. In the experimental data shown in this figure, a transition region between the zone of flow establishment and the established flow region is observed. Indicating that the established flow region began at approximately 6 diameters downstream from the exit of the jet (see Figure 9). The centerline concentration decay shows a change in the decay rate of the axial concentration, which begins at the location corresponding to the maximum lateral penetration, for instance. This axial distance was defined as x_b. It would appear that at this point the overall behavior changes from a free jet regime to a mixing stagnation region. In the mixing region the counterflow stream is considered to be the dominant flow. This transition region can be also observed in Figure 8.

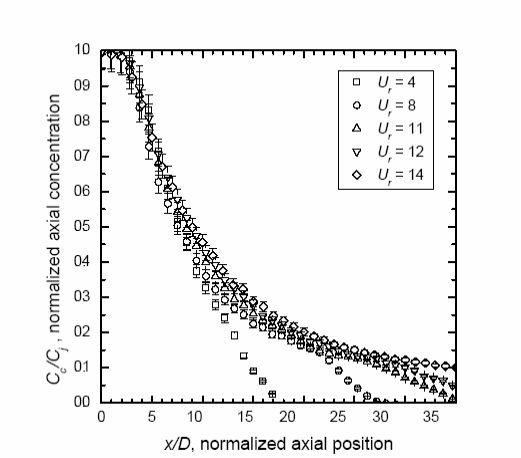

Figure 7: Centerline mean concentration decay

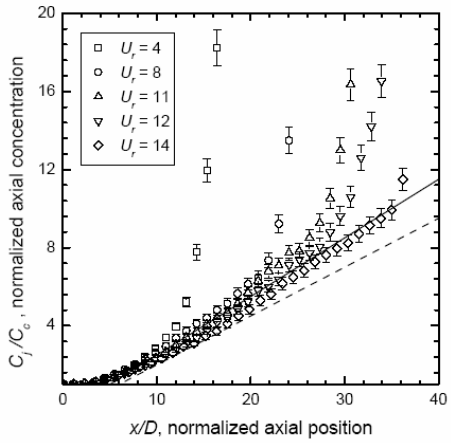

Figure 8: Centerline mean concentration dilution.(Dashed line: 0.25 slope found by Yoda and Fiedler (1996) and solid line: 0.3 slope found in the present study.

The dilution of the centerline concentration of the counterflowing jet with nozzle D_1 is shown in Figure 8. In this figure the inverse of the normalized mean axial concentration decay (C_j/C_c) is plotted against the normalized axial location (x/D). Profiles of the dilution in the centerline of the jet are obtained for jet to counterflowing velocity ratios: 4, 8, 11, 12, and 14. The dashed line in the graph shows the 0.25 slope experimentally found by Yoda and Fiedler (1996) for $x/D < 10$. However, for a larger downstream distance, a slope of 0.30 (solid line) seems to be more representative of the dilution for the mean centerline concentration. Nevertheless, it is evident that in the counterflowing jet the dilution of the centerline occurs faster than the jet in a quiescent stream for which the slope is found to be about 0.20 (Dahm and Dimotakis, 1990).

Lam and Chan (2002) suggested that a rough collapse of the data into a single curve is observed if C_j/C_c is plotted against x/x_p. With the data available in this investigation, the collapse of the profiles into a single curve was not observed. Figure 8 shows that the dilution of the mean concentration is stronger for the low value of U_r, on the other hand, when the velocity ratio U_r is higher, the dilution in the axial concentration resembles the dilution for a free jet.

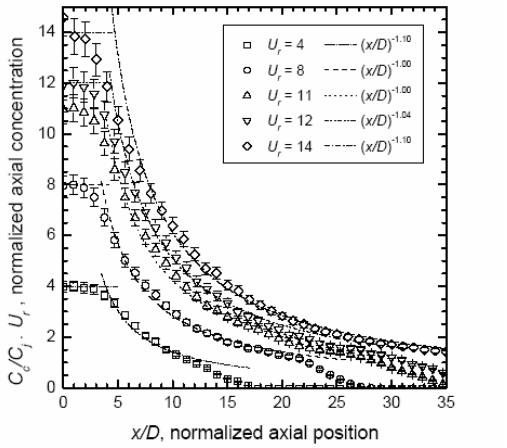

Figure 9: The normalized centerline mean concentration.

Mean concentration values along the axis of the jet are plotted in Figure 9. In this figure the value of the axial concentration is normalized by the concentration at the exit of the jet (C_j) scaled by the velocity ratio, and plotted against the normalized axial position of the jet. The axial position along the axis of the jet was normalized by the diameter of the jet. Figure 9 shows the variation of the jet penetration with U_r.

Table 2: Penetration distance, length of the established flow region, and lateral penetration of 5 % contour of the jet.

D	U_r	x_p/D	y_p/D	y_p/x_p	x_b/x_p
8.81	4	16.50	4.21	0.26	0.60
"	8	25.00	6.50	0.24	0.68
"	11	31.67	7.09	0.22	0.69
"	12	34.75	7.56	0.22	0.71
"	14	42.00	9.44	0.23	0.70
5.64	8	20.25	5.50	0.27	0.66
"	11	27.25	5.94	0.24	0.66
"	14	31.50	7.50	0.24	0.76
"	16	43.75	8.38	0.19	0.75
"	19	51.50	6.88	0.13	0.71

The scaled concentration profiles depict in an easier manner the "free jet-like" region, for which the counterflowing jet behaves similar to an ordinary jet (Konig and Fiedler, 1991b; Beltaos et al., 1999; Yoda and Fiedler, 1996). This free jet-like region is defined as the region for which the jet flow is the dominant flow, and its length extends up to approximately 70 % of the total penetration length of the jet (Lam and Chan, 2002). Data collected show that the length of the free jet-like region coincides in most of the experiments with the axial position of the maximum lateral penetration of the jet x_b. The average value of x_b was found to be 69 % of the total penetration length of the jet; the corresponding data can be seen in Table 2.

Beltaos and Rajaratnam (1973) suggested that the measurements of the center line velocity decay of the counterflowing jet collapse on to a single curve for $U_r > 4$ when the axial velocity is plotted using the form

$$\frac{U+U_o}{U_j}\frac{x_p}{D} = f(\frac{x}{x_p}) \qquad (1)$$

Where U is the centerline value of the velocity. This equation indicates that the maximum penetration length of the counterflowing jet can be used as the length scale of the centerline concentration decay. However, for the case of the concentration field, the concentration of the counterflow stream is zero. Therefore, Equation 1 is written as

$$\frac{C_x}{C_j}\frac{x_p}{D} = f(\frac{x}{x_p}) \qquad (2)$$

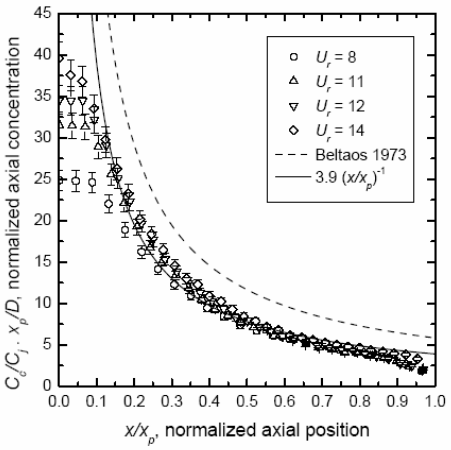

Figure 10: Centerline concentration decay of the counterflowing jet plotted using the universal form presented by Beltaos and Rajaratnam (1973) for the centerline velocity decay of a jet in a counterflow stream.

Figure 10 depicts the centerline concentration profiles for the counterflowing jet represented by Equation 2. It shows that the universal form of the axial concentration decay for the counterflowing jet is a good representation for $x/x_p > 0.5$ (50 % of the jet penetration). Beltaos and Rajaratnam (1973) indicated that for $U_r > 4$, the data follow a decay proportional to x^{-1}. The function presented by Beltaos and Rajaratnam (1973) is also shown in Figure 10. It is important to mention that the function given by Beltaos and Rajaratnam (1973) was generated using the velocity, therefore, this function should not follow the data of the concentration field, the best fit of the data is given by

$$\frac{C_x}{C_j}\frac{x_p}{D} = 3.9(\frac{x}{x_p})^{-1} \qquad (3)$$

The centerline concentration is proportional to x^{-1} as can be observed in figures 9 and 10. Even though the curve described in Equation 3 shows a better fit for the data, it collapses nice into a single curve for $x/x_p > 0.5$. Figure 11 shows that the experimental data of the centerline concentration decay collapses into a single curve just for $x > 0.5x_p$. Similar results were found in the investigation presented by Chan and Lam (1998). In this investigation was indicated that the centerline velocity decay collapses into a single curve for a short part of the total jet penetration of the counterflowing jet when it was plotted using equation 1. Therefore, the universal form of the centerline velocity decay is valid for values of x within this range. Although, the function given by equation 2 does not represent a universal curve of the centerline concentration decay it is clear that axial concentration decays proportional to x^{-1} for the range of U_r studied in this investigation.

The maximum half-width of the 5 % contour can be considered as an important scale for the centerline concentration decay. For a conserved scalar would be logical to expect that a higher lateral spread rate would result in a steeper decay in the centerline concentration. To test this, the maximum half-width of the 5 % contour (y_p) was used instead of the maximum axial penetration length (x_p) in equation 2. Figure 11 shows the data of the nozzle of diameter D_1 plotted using the form

$$\frac{C_x}{C_j}\frac{y_p}{D} = f\left(\frac{x}{x_p}\right) \qquad (4)$$

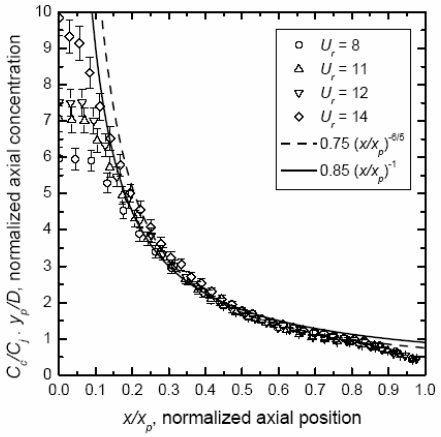

Figure 11: Centerline concentration decay of the counterflowing jet plotted using the modifed version of the universal form presented by Beltaos and Rajaratnam (1973) for D_1.

Figure 11 shows the data for the centerline concentration decay collapsing into a single curve for $x/x_p > 0.2$. The collapsing range of the centerline concentration shown in this figure is significantly larger than the one observed in figure 10.

The universal form given by equation 4 was found to be valid just for a limited range of U_r.

As can be seen in figures 11 and 12, this range is limited by $8 < U_r < 16$. It is clear from figure 12 that the trend of data for $U_r = 19$ does not drop into the same curve as is the case of $U_r < 19$. Additionally, it is possible to observe that the equation of the similar curve is not the same as the one as in figure 11. The similar region shown in this figure is found to be valid for an axial distance in the range of $0.2 < x < 0.7$. Within this region, the decay of the centerline concentration was determined to be proportional to $x^{-6/5}$. However, a decent approximation of the axial decay is obtained if the centerline concentration is considered to decay with x^{-1}, which can be seen in figure 12.

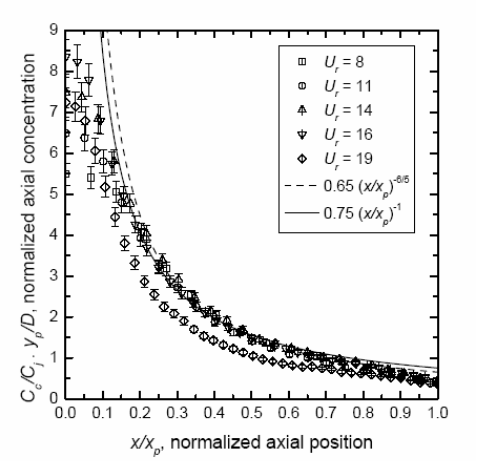

Figure 12: Centerline concentration decay of the counterflowing jet plotted using the modifed version of the universal form presented by Beltaos and Rajaratnam (1973) for D_2.

The fact that the universal form given by equation 4 is not valid for $U_r = 19$ can be explained by looking at the value of the maximum half-width lateral penetration (y_p). From Table 2 it is possible to observe that for $U_r = 19$ the value of y_p shows a sudden drop, affecting the similarity of the concentration profiles in Figure 12. This suggests that y_p is not the ideal scale for the centerline concentration decay. This would suggest that a relation of the maximum half-width penetration and the maximum axial penetration would be better suited scales for the centerline concentration decay in a counterflowing jet.

Table 3 contains the different length ratios for some of the performed experiments. These ratios were used to generate several self similar curves of the centerline concentration decay for the counterflowing jet. In order to simplify the notation new parameters were defined, these are, λ, β, and φ, which correspond to y_p/x_b, y_p/x_p, and x_b/x_p respectively. Using these new parameters, it was possible to define new axial distances, for instance x_λ was defined as the axial position for which the center-line concentration was equal to λ times the concentration at the exit of the nozzle of the jet. In similar form the axial distances x_β and x_φ were also defined.

Figure 13 and Figure 14 show the centerline profiles of the concentration decay for the counterflowing jet when these are plotted using the parameters λ and β as the scale of the centerline concentration decay. These profiles were obtained

Table 3: Geometrical scale length using the jet penetration (x_p), maximum half-width lateral penetration (y_p), and the axial location of the maximum lateral penetration (x_b).

D	U_r	y_p/x_b	y_p/x_p	x_b/x_p
8.81	4	0.4	0.26	0.60
"	8	0.35	0.24	0.68
"	11	0.32	0.22	0.69
"	12	0.31	0.22	0.71
"	14	0.32	0.23	0.70
5.64	8	0.41	0.27	0.66
"	11	0.36	0.24	0.66
"	14	0.31	0.24	0.76
"	16	0.25	0.19	0.75
"	19	0.19	0.13	0.71

using the parameters λ and β instead of x_p/D in equation 2. Figure 13 shows that for velocity ratios equal or higher than 8, the different centerline concentration profiles collapse into a single curve independent of the initial conditions of the jet. In these figures it is possible to observe that the centerline concentration decays with $x^{-6/5}$.

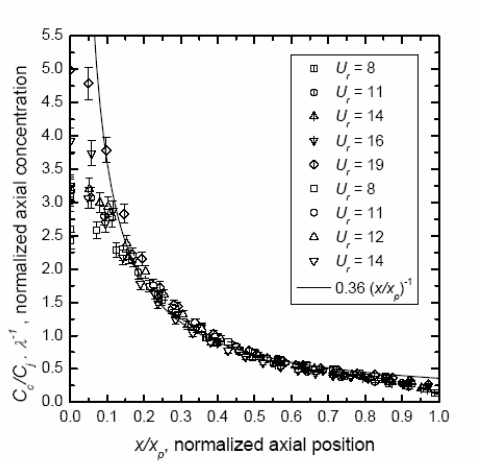

Figure 13: Centerline concentration profiles of the counterflowing jet (open symbols correspond to D1 and the crossed symbols to D2).

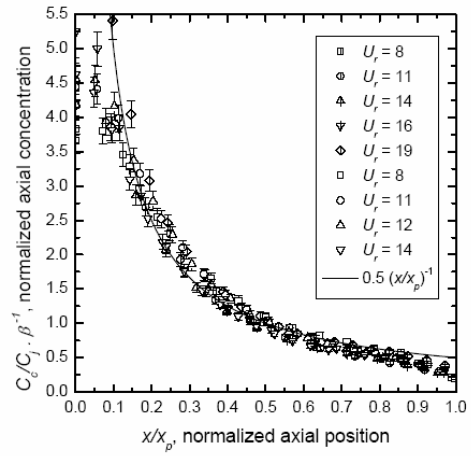

Figure 14: Centerline concentration profiles of the counterflowing jet. (open symbols correspond to D1 and the crossed symbols to D2).

Nevertheless, similar to the case depicted in Figures 11 and 12 the axial decay can be approximated by considering decay proportional to x^{-1}. Therefore, it is possible to suggest that the use of λ as a scale for the axial concentration decay offers better results than by using y_p/D and x_p/D. It is important to mention that the data that most departs from the fitted curve corresponds to U_r =14 for which the penetration length x_p was estimated and not experimentally measured, because this axial penetration was out of the range of the camera field of view.

A similar behavior of the centerline concentration is observed in figure 14. It can be seen that the scatter of the data when β is used as the scaling factor is significantly higher than for the case of λ. However, the trends of data in figure 14 demonstrate a similar shape for the different jet-to-counterflowing velocity ratios.

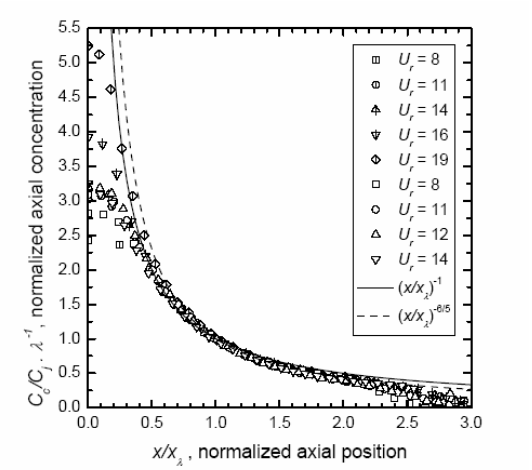

Figure 15: Centerline concentration profiles of the counterflowing jet.

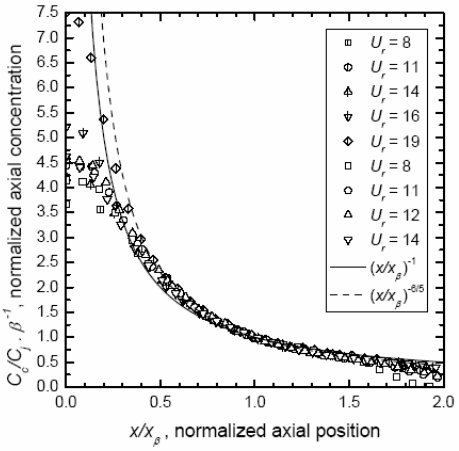

Figure 16: Centerline concentration profiles of the counterflowing jet.

It is clear from figure 14 that the centerline decay for the counterflowing jet is proportional to the inverse of the axial distance.The parameters λ and β were used to define forms for which the centerline concentration profiles show a similar behavior within the established flow region.

Figures 15 and 16 show the data of the axial concentration profile collapsing on a single curve. In these figures, the location of the concentration along the axis of the jet was normalized by the axial distance where the normalized centerline concentration was equal to λ and β times the concentration at the exit of the jet, for figures 15 and 16 respectively. In these figures the normalized centerline concentration decay was scaled by the inverse of the length ratios λ and β. Figures 15 and 16 depict the centerline concentration decay of a counterflowing jet collapsing very nicely onto a single curve. It is possible to see that the decay of the axial concentration can be considered to be inversely proportional to the axial distance x. However, it was found that this concentration decay is better predicted by $x^{-6/5}$, shown as a dashed line in figures 15 and 16. From the experimental data studied in this investigation the established flow region was found to be located at approximately 6D downstream of the exit of the jet. At approximately 6D, the concentration value of the jet was about 70 % of the concentration at the nozzle, therefore, it is possible to state that the form of the centerline concentration shown in figure 15 and figure 16 is valid for a significant portion of the zone of established flow. This dimensionless form of the axial concentration fits the experimental data for concentration values between 85 to 11 % of the concentration at the exit of the jet. Note that the zone of established flow is not found immediately after the iso-concentration core zone, in fact, there is a transition region between the iso-concentration core and the zone of established flow (Chan and Lam, 1998).

The parameter φ was also used to generate a universal form of the centerline concentration decay for the counterflowing jet, in a similar way that λ and β were used; the results of which can be observed in figure 18. It can be seen that similar to the outcomes obtained in figure 15 and figure 16, the axial concentration decay for the different jet to counterflowing velocity ratios collapsed onto a single curve. Nonetheless, this novel form for the centerline concentration was proven to be conditional upon the inlet condition, since the same result was not obtained for the case of the smaller jet diameter. Therefore, only the results obtained for the larger jet diameter are shown in figure 17.

Another function form for which the centerline concentration decay shows a similarity region was proposed by Lam and Chan (1995). It was suggested that the stagnation surface or dividing surface, as was defined by the authors, was located at the brightness contour for which $L_p = e^{-1}L_m$, where L_m was considered to be the maximum intensity level at the center of the "bright patch" observed in the experiments of this investigation, and was located approximately at the center of the concave shape of the stagnation surface. It is important to point out that the work of Lam and Chan (1995) had similar intent, however, they did not base their findings on calibrated concentration measurements, but on light intensity. The light intensity observed is not directly proportional to scalar concentration as it may be biased by pixel sensitivity, camera field non uniformity and high laser sheet heterogeneity. However, there is a difference between the criterion presented by Lam and Chan (1995) and the one used in this study. Instead of using the location of the intensity contour where the intensity was equal to e^{-1} times the intensity of the "bright patch", we used the location for which the centerline concentration was equal to e^{-1} times the concentration at the exit of the jet. This axial position was defined as $x_{1/e}$. Figure 18 depicts the centerline concentration decay of the counterflowing jet against the axial position normalized by the parameter $x_{1/e}$.

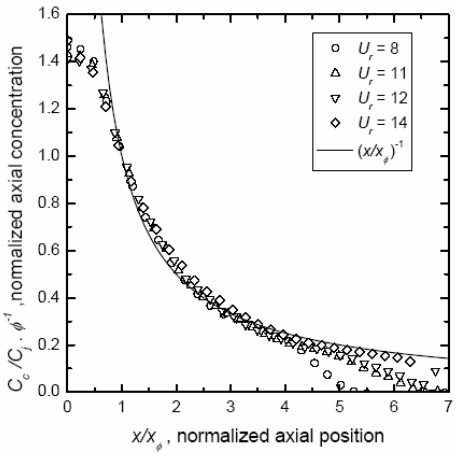

figure 17: Centerline concentration profiles of the counterflowing jet. Experiments correspond for D_1.

It can be seen that the axial concentration profiles for different U_r are similar when the axial position of the centerline concentration is normalized by $x_{1/e}$ for U_r greater than 4. In Figure 18 we can observe that a single power law fits relatively well to the experimental data. It is possible to state that the normalized concentration follows the function

$$\frac{C_c}{C_j} = 0.35\left(\frac{x}{x_{1/e}}\right)^{-1} \qquad (5)$$

In order to completely define the centerline concentration decay for the counterflowing jet, it is important to discus how the new parameters (λ, β) and the new axial distances (x_λ, x_β, and $x_{1/e}$) are related with the jet to counterflowing velocity ratio.

Figure 19 shows the variations of λ and x_λ with U_r. A linear regression was performed and it was found that the available data responded to a linear relation with U_r. The correlation coefficient found for both the linear regressions were 0.95 and 0.91 for the case of λ and x_λ respectively. It is important to mention that the linear fit obtained for x_λ was forced to go through zero in order to satisfy the physical meaning of this parameter. It can be seen that most of the data drops into the 95 % confidence line shown in figure 19 (dashed line).

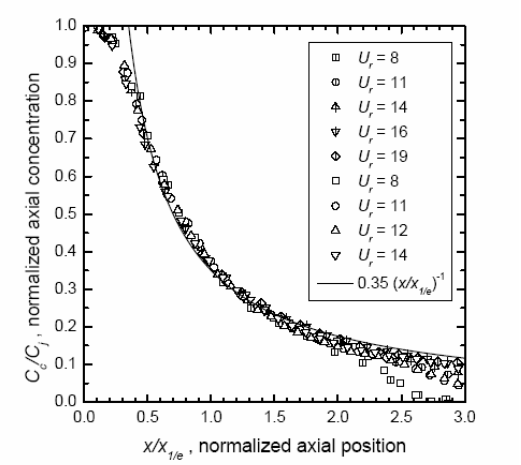

Figure 18: Centerline concentration profiles of the counterflowing jet (open correspond to D1 and the crossed symbols to D2).

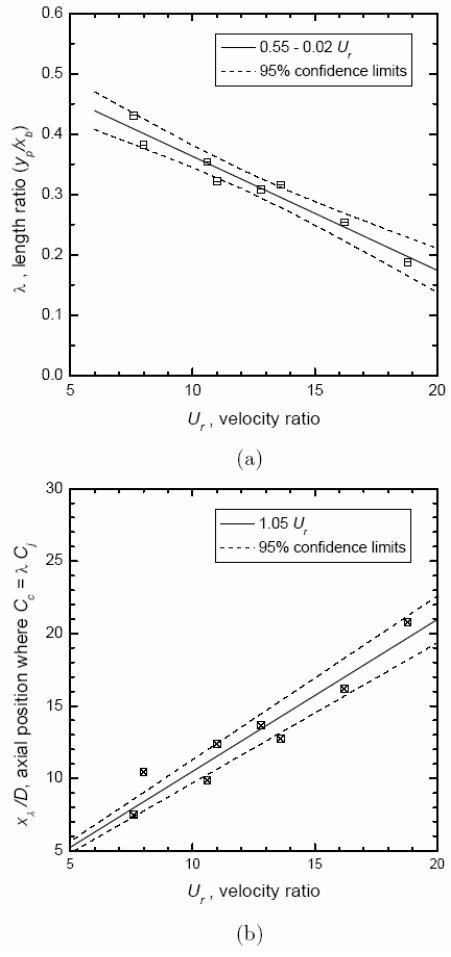

Figure 19: Variation of the new parameters λ *(a)* and x_λ *(b)* with U_r.

Figure 20 depicts the parameters β and x_β as function of U_r. It can be appreciated that the data shown in this graph can be approximated by a linear function of U_r. The R^2 found for the function that represents a β and x_β were found to be 0.90 and 0.88 respectively.

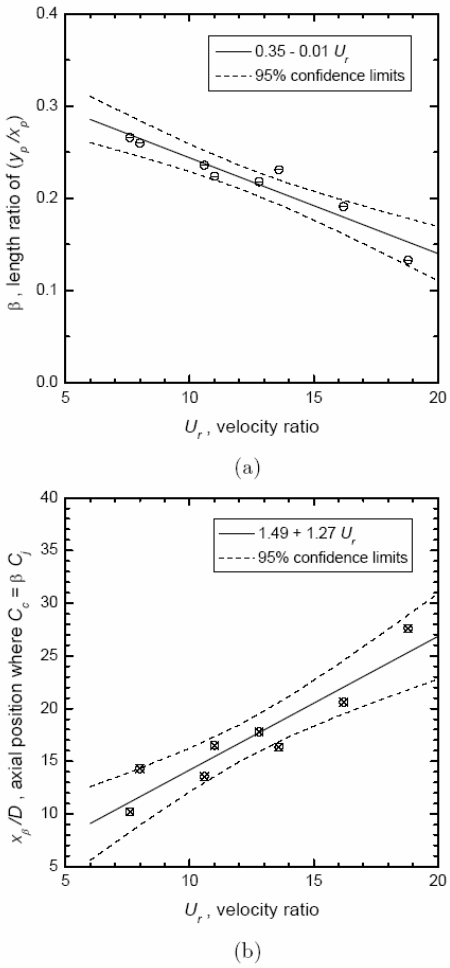

Figure 20: Variation of the new parameters β(a) and x $_\beta$ (b) with U_r.

It can be seen from figure 20a that a nonlinear fit can be used to better represent the parameter β as a function of U_r. However no significant improvement in the prediction of the centerlines concentration was observed when using a nonlinear fit (data not presented in this investigation). Similar to x_λ and x_β, the axial position $x_{1/e}$ was found to have a linear dependance on U_r, as can be seen on figure 21. This linear fit has a R^2 of 0.90, therefore it is possible to state that this linear relation represents the real data relatively well.

Since λ, β, x_λ, x_β, and $x_{1/e}$ can be related with U_r, experimental equations can be generated in order to predict the centerline concentration decay for the counterflowing jet. The experimental expressions are valid for the free jet-like region up to approximately 0.70 x_p. From figures 15, 16, and 18 it is possible to write the centerline concentration decay in the forms

$$\frac{C_c}{C_j} = \lambda\, x_\lambda (\frac{1}{x}) \qquad (6)$$

$$\frac{C_c}{C_j} = \beta\, x_\beta (\frac{1}{x}) \qquad (7)$$

$$\frac{C_c}{C_j} = 0.35\, x_{1/e} (\frac{1}{x}) \qquad (8)$$

Figures 19, 20, and 21 showed that, λ, β, x_λ, x_β, and $x_{1/e}$ can be written as a function of U_r. Therefore equations 6, 7, and 8 can be expressed as

$$\frac{C_c}{C_j} = (0.55 - 0.02\,U_r)(1.05\,U_r)\, D\, (\frac{1}{x_o + x}) \qquad (9)$$

$$\frac{C_c}{C_j} = (0.35 - 0.01\,U_r)(1.49 + 1.27\,U_r)\, D\, (\frac{1}{x_o + x}) \qquad (10)$$

$$\frac{C_c}{C_j} = 0.35\,(6.91 + 0.3\,U_r)\, D\, (\frac{1}{x_o + x}) \qquad (11)$$

x_o represents the axial distance at which the effects of the iso-concentration core can be neglected. It was observed that the value of x_o varies with the jet to counterflow velocity ratio U_r. However, the proper value of x_o can be easily computed by finding a x_o that produced C_c/C_j equal to 1 for x equal to zero. In order to validate equations 9, 10, and 11 experiments at U_r = 8 and U_r = 11 were repeated using the nozzle with a diameter equal to 8.814 mm and the equations were used to predict the centerline decay of the counterflowing jet at these flow conditions.

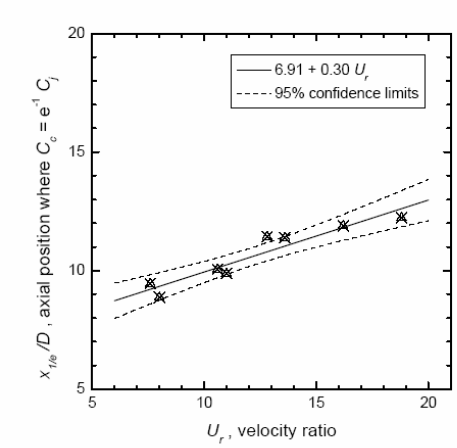

Figure 21: Axial distance $x_{1/e}$ as a function of U_r.

Figure 22 depicts the experimental data of the centerline concentration decay of a counterflowing jet with U_r = 8 and diameter 8.814 mm. The predicted value of the axial concentration decay using equations 9, 10, and 11 are also shown in this figure. The predicted values of C_c using the empirical equations seem to follow well the experimental data for the same flow conditions. The error bars shown in figure 22 correspond to the 10 % error using equation 9, which best predicts the experimental data. The same prediction is found when equation 11 is being used.

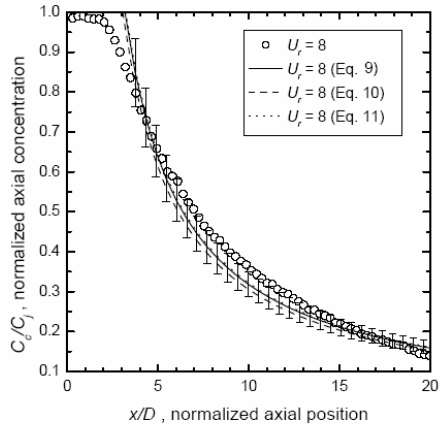

Figure 22: Centerline concentration decay for a counterflowing jet with U_r = 8.

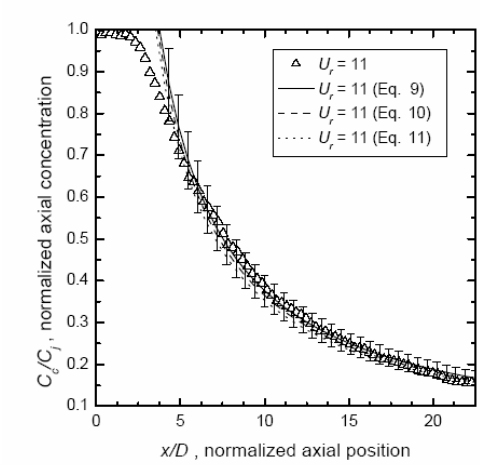

Figure 23: Centerline concentration decay for a counterflowing jet with U_r = 11.

The prediction of the centerline concentration decay improves at higher jet to counterflow velocity ratio, which can be appreciated in figure 23. The data shown in this figure are significantly well predicted by any of the above equations, nonetheless, it is easily to observe that equation 9 shows the best prediction of the results. The error bars in the graph correspond to the 10 % error of the predicted value using equation 9. From the previous discussion, it is possible to suggest that any of these equations can be used to predict the centerline concentration decay for a counterflowing jet for at least the range of U_r tested in the present investigation.

SUMMARY

The centerline concentration decay of a round jet issuing into a uniform counterflowing stream has been investigated using planar laser induced fluorescence. The application of the axial penetration x_p as the scaling length of the mean concentration

field has been investigated. Additionally, two forms of the aspect ratio of the 5 % contour and the axial distance $x_{1/e}$ were used as length scales for the centerline concentration decay. The following conclusions were drawn from the quantitative study of these length scales:

1. It was observed that the maximum axial penetration of the counterflowing jet generated a similar form of the centerline concentration for $x/x_p > 0.5$ (greater than 50 % of the jet penetration).
2. The new scaling factors λ and β were found to produce a universal form of the centerline concentration decay. The scaling factors were defined based on the aspect ratio of the 5 % contour of the mean concentration field of the counterflowing jet.
3. The simple empirical equations developed in this investigation were found to predict relatively well the centerline concentration decay in the established flow zone.

ACKNOWLEDGMENTS

This work was supported by the Natural Sciences and Engineering Research Council of Canada (NSERC).

REFERENCES

1. Arendt, J., Babcock, H. A., and Schuster, J. C. (1956). Penetration of a jet into counterflow. *Proc. ASCE Journal Hydraulics Division 82,* pages 1038 - 8 - 11.
2. Beltaos, S., Brinkworth, B. J., Lam, K. M., and Chan, H. C. (1999). Round jet in ambient counterflowing stream. *Journal of Hydraulic Engineering,* 125(4):428 -432.
3. Beltaos, S. and Rajaratnam, N. (1973). Circular turbulent jet in an opposing infinite stream. *First Canadian Hydraulics Conference, Edmonton.*
4. Bernero, S. and Fiedler, H. E. (2000). Application of particle image velocimetry and proper orthogonal decomposition to the study of a jet in a counterflow. *Experiments in Fluids,* pp. S274 - S281.
5. Chan, H. C. (1999). *Investigation of a round jet into a counterflow.* PhD thesis, Dept. of Civil Engineering, University of Hong Kong.
6. Chan, H. C. and Lam, K. M. (1998). Centerline velocity decay of a circular jet in a counterflowing stream. *Physics of Fluids,* 10(3):637 - 644.
7. Dahm, W. J. A. and Dimotakis, P. E. (1990). Mixing at large schmidt number in the self-similar far field of turbulent jets. *Journal of Fluid Mechanics,* 217:299 - 330.
8. Hilderman, T. L. (2004). *Measurement, modelling, and stochastic simulation of concentration fluctuations in a shear flow.* PhD thesis, University of Alberta.
9. Konig, O. and Fiedler, H. E. (1991a). On the asymptotic behaviour of axisymmetric turbulent jets in an ambient stream under arbitrary inclination angles. *Zeitschrift filr Flugwissenschaften und Weltraumforschung,* 15(2): 103 - 106.
10. Konig, O. and Fiedler, H. E. (1991b). The structure of round turbulent jets in counterflow: a flow visualization study. *Advances in turbulence 3,* pages 61 - 66.
11. Lam, K. M. and Chan, C. H. C. (2002). Time-averaged mixing behavior of circular jet in counterflow: Velocity and concentration measurements. *Journal of Hydraulic Engineering,* 128(9):861 - 865.
12. Lam, K. M. and Chan, H. C. (1995). Investigation of turbulent jets issuing into a counterflowing stream using digital image processing. *Experiments in Fluids,* 18:210 -222.
13. Lam, K. M. and Chan, H. C. (1997). Round jet in ambient counterflowing stream. *Journal of Hydraulic Engineering,* 123(10):895 - 903.
14. McDannel, M. D., Peterson, P. R., and Samuelsen, G. S. (1982). Species concentration and temperature measurements in a lean premixed flow stabilized by a reverse jet. *Combustion Science and Technology,* 28:211 - 224.
15. Morgan, W. D. and Brinkworth, B. J. (1976). Upstream penetration of an enclosed counterflowing jet. *Industrial and Engineering Chemistry Fundamentals,* 15(2):125- 127.
16. Powell, I. (1987). Design of a laser beam line expander. *Applied Optics,* 26(17):3705- 3709.
17. Rajaratnam, N. (1976). *Turbulent jets,* volume 5 of *Developments in Water Science.* Elsevier Science Ltd.
18. Sui, K. N. (1961). The investigation of the development of circular and planar jets in parallel and opposing streams. *Eesti NSV teaduste akadeemia, Tallin, Toime-tised, Isvestia Fuusika - matemaatika - ja technikateaduste seeria. Seeria fiziko - matimaticheskikh nouk.,* 10:215 - 223.
19. Timma, E. (1962). Turbulent circular and falt streams developing in a counterflow. *Russian periodical, Adakemii Nauk. Estonskoy SSr, Seriya Fiziko - Matamatich-eskikh i Tekhnicheskikh Nauk,* 4:253 - 262.
20. Tsunoda, H. and Saruta, M. (2003). Planal laser-induced fluorescence study on the diffusion field of a round jet in a uniform couter-flow. *Journal of Turbulence,* 4(013).
21. Yoda, M. and Fiedler, H. E. (1996). The round jet in a uniform counterflow: flow visualization and mean concentration measurements. *Experiments in Fluids,* 21(6):427 -436.